ACS APPLIED MATERIALS & INTERFACES

Research Article

www.acsami.org

Solvothermal-Induced Conversion of One-Dimensional Multilayer Nanotubes to Two-Dimensional Hydrophilic VO_x Nanosheets: Synthesis and Water Treatment Application

Ren Cai,[†] Jing Chen,[‡] Dan Yang,[‡] Zengyi Zhang,[‡] Shengjie Peng,[‡] Jin Wu,[‡] Wenyu Zhang,[‡] Changfeng Zhu,[‡] Tuti Mariana Lim,[∥] Hua Zhang,[‡] and Qingyu Yan*[,‡,§,⊥]

[†]Department of Chemistry, University of Florida, Gainesville, Florida 32611, United States

[‡]School of Materials Science and Engineering, Nanyang Technological University, 50 Nanyang Avenue, Singapore 639798, Singapore

[§]TUM CREATE Centre for Electromobility, Nanyang Technological University, Singapore 637459, Singapore

[∥]School of Civil and Environmental engineering, Nanyang Technological University, Singapore 639798, Singapore

[⊥]Energy Research Institute@NTU, Nanyang Technological University, Singapore 637459, Singapore

Supporting Information

ABSTRACT: Ultrathin 2D nanostructures have shown many unique properties and are attractive for various potential applications. Here, we demonstrated a strategy to synthesize ultrathin VO_x nanosheets. The as-obtained ultrathin VO_x nanosheets showed a large Brunauer–Emmett–Teller (BET) surface area of 136.3 m^2g^{-1}, which is much larger than that of 1D multilayer VO_x nanotubes. As a proof of concept, these hydrophilic ultrathin nanosheets were applied in water treatment and exhibited excellent absorption capability to remove Rhodamine B (RhB) in wastewater owing to their large specific surface area, good hydrophilic property, and more negative zeta potential. In addition, this method could be generalized to prepare other 2D nanostructures with great potential for various attractive applications.

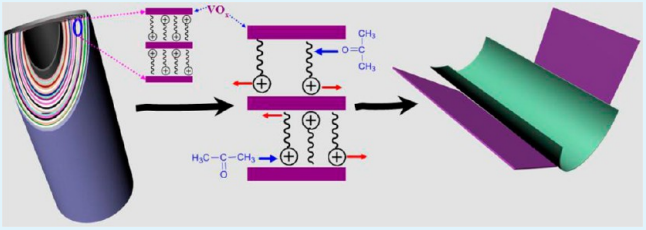

KEYWORDS: *ultrathin VO_x nanosheets, multilayer VO_x nanotubes, water treatment application*

INTRODUCTION

Two-dimensional (2D) nanostructures of metal oxides and semiconductors have attracted tremendous attention because of their interesting properties related to their structures. Particularly, ultrathin nanosheets (thickness of <5 nm) with lateral dimension of up to micrometers are regarded as an important new type of material, due to their exceptionally high specific surface area and potential applications in electronics,[1,2] sensors,[3,4] catalysis,[5,6] and energy-storage devices.[7] Great research effort has been devoted to preparing novel ultrathin 2D nanostructures of various materials.[8−12] For instance, free-standing semiconductor CdSe nanosheets with a thickness of 1.4 nm were synthesized through a soft colloidal template method.[13] Ultrathin, single-crystalline ceria nanosheets with a thickness of approximately 2.2 nm and lateral dimension up to 4 μm were obtained by an aqueous route.[14] A freestanding form of ultrathin hexagonal palladium nanosheets was reported by using a CO-confined growth method.[15] Metallic few-layered VS_2 ultrathin nanosheets were prepared in an all-in-solution route.[16] New methods with simple steps are always encouraging in this research field.

Herein, we report a simple approach of synthesizing ultrathin VO_x nanosheets (the compound of VO_2 and V_2O_5) through opening of nanotubes. The study indicates that the mutual diffusion processes of acetone and dodecylamine are the key to expand 1D multilayer VO_x nanotubes to form the nanosheets as illustrated by the scheme in Figure 1. The ultrathin VO_x nanosheets with thickness of 1.2−5.3 nm and a large specific surface area of 136.3 m^2 g^{-1} can be synthesized on a large scale at relatively low temperatures (120 °C). Taking advantage of the large surface area and hydrophilic characteristics, we tested these nanosheets in pollution treatment applications. The sample exhibited an excellent absorption ability to remove Rhodamine B (RhB) in water.

EXPERIMENTAL SECTION

Materials. Crystalline V_2O_5 powder (99.9%, Sigma-Aldrich), hydrogen peroxide solution (H_2O_2, 30%, Sigma-Aldrich), dodecylamine ($CH_3(CH_2)_{11}NH_2$, ≥99%, Sigma-Aldrich), Rhodamine B (RhB, $C_{28}H_{31}ClN_2O_2$, 99%, Sigma-Aldrich), and acetone (95%, Sigma-Aldrich) were used. All the materials were used without further purification.

Synthesis of 1D Multilayer VO_x Nanotubes. In a typical experiment,[17] crystalline V_2O_5 powder (1.0 g) was added to hydrogen peroxide solution (80 mL, 30%) under magnetic stirring for about 30

Received: August 23, 2013
Accepted: September 27, 2013
Published: September 27, 2013

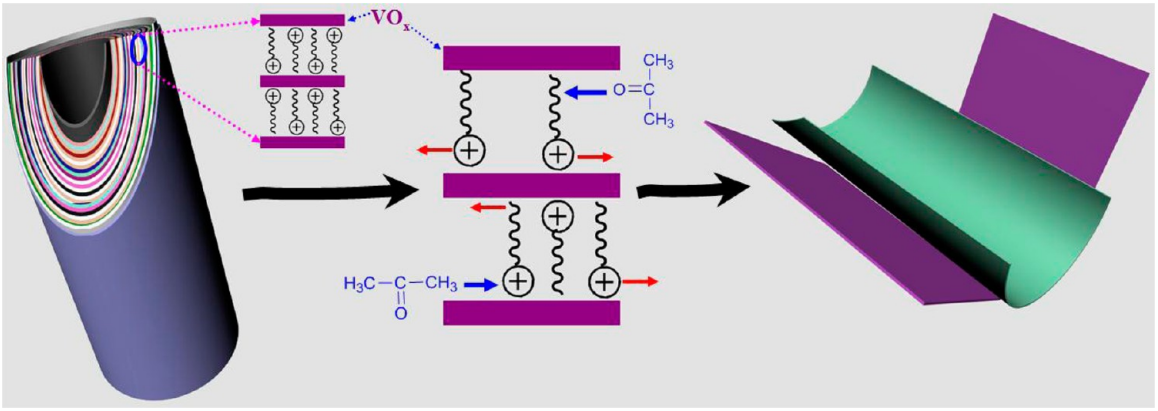

Figure 1. Schematic of the transformation from 1D multilayer nanotubes to 2D ultrathin nanosheets.

min. Then, a following strong exothermic reaction in the solution led to the formation of clear orange vanadium peroxide sol and become red gel. After that, 1.0 g of dodecylamine was added to the orange solution. The mixture was vigorously stirred for 20 min and transferred into a 100 mL Teflon-lined stainless steel autoclave. The autoclave was finally sealed and placed in an electric oven at 180 °C for 5 days.

Synthesis of 2D Ultrathin VO_x Nanosheets. An amount of 4.2 mg of as-prepared multilayer VO_x nanotubes was dispersed in 40 mL of acetone (99.9%) under ultrasound for 60 min in a 50 mL Teflon autoclave (actual volume of the autoclave was about 46.4 mL). The temperature of the water bath of the ultrasound is about 40 °C. Then, 6.4 mL of acetone was added into the autoclave to cover the whole volume and maintained at 120 °C for 7 h. The final products were washed by acetone and methanol followed by centrifugation at 8500 rpm for 10 min several times.

Materials Characterization. The morphology of the samples was characterized with a field emission scanning electron microscope (FESEM) system (JEOL, model JSM-7600F) and a transmission electron microscope (TEM) system (JEOL, Model JEM-2010F) operating at 200 kV. Crystal phases of the samples were investigated using a Bruker D8 Advance diffractometer X-ray diffraction (XRD) at the 2θ range of 10° to 80° with Cu Kα radiation. Fourier transform infrared spectroscopy (FTIR) measurements were conducted in a Perkin-Elmer Instruments Spectrum GX FTIR spectrometer at room temperature from 400 to 4000 cm^{-1}. A total of 32 scans were recorded at a resolution of 2 cm^{-1} for averaging each spectrum. X-ray photoelectron spectroscopy (XPS) of the resulting composites was performed with an X-ray photoelectron spectrometer (Kratos AXIS Ultra) using monochromatic Al Kα (1486.71 eV) X-ray radiation (15 kV and 10 mA); 160 eV pass energy was used for the survey scan, whereas 40 eV was used for the high-resolution scan. The specific surface area was calculated by the Brunauer–Emmett–Teller (BET) method using nitrogen adsorption/desorption (Quantachrome Instruments, Autosorb AS-6B), and atomic force microscopy (AFM) (Digital Instruments) was used to determine the thickness of the VO_x nanosheets. The contact angle measurements of the samples are measured on a THETA Optical Tensiometer (KSV Instrument Ltd., Finland).

RESULTS AND DISCUSSION

The synthesis steps start with the preparation of a multilayer VO_x nanotube by a hydrothermal reaction process (see Experimental Section). The morphologies and structures of the products were characterized by using field emission scanning electron microscopy (FESEM) and transmission electron microscopy (TEM). The SEM images (see Supporting Information Figure S1a,b) reveal that the products were uniform tubular structures with average length of ~2 μm and diameters in the range of 40–60 nm. Crystal phases of VO_2 (B) (JCPDS: 31-1439) and orthorhombic V_2O_5 (JCPDS: 03-0206) can be identified in the corresponding powder X-ray diffraction (XRD) pattern in Figure S1c (Supporting Information). The low-magnification TEM image (see Supporting Information Figure S1d) clearly displays the hollow feature of these nanotubes (Note: VO_x nanotubes). The high-magnification TEM image (see Supporting Information Figure S1e) further indicates that these tubes are open-ended with multilayered walls. The high-resolution TEM (HRTEM) image of some cross-section region reveals the thickness of each layer is ~1.3 nm (see Supporting Information Figure S1f,e). The top-view HRTEM image (see Supporting Information Figure S1g) of one single VO_x nanotube indicates that it is polycrystalline, which is confirmed by the ring pattern of the selected area electron diffraction (SAED) pattern (see inset in Figure S1g, Supporting Information). A side-view HRTEM image of one layer in the tubes shows that the lattice spacing of 0.21 nm corresponds to the (110) planes of orthorhombic V_2O_5. The X-ray photoelectron spectroscopy (XPS) analysis (see Supporting Information Figure S2) shows that the V 2p3/2 band can be fitted into two peaks at 517.6 eV (V^{5+}) and 516.3 eV (V^{4+}). Calculated from the peak area, the molar ratio of V^{5+}/V^{4+} is estimated to be 2.44. This means that the surface region of the multilayer VO_x nanotubes was composed of mixed phases of V_2O_5 and VO_2 with a molar ratio of 1.22; i.e., x is about 2.35.

These presynthesized multilayer VO_x nanotubes were dispersed in the acetone by ultrasound for 1 h and kept at 120 °C for 7 h. The morphology of the sample is shown in Figure 2. The SEM images (Figure 2a,b) reveal that the typical lateral dimension of the nanosheets ranges from hundreds of nanometers to several micrometers. The surfaces of the nanosheets are smooth. XRD pattern shows that the sample remains as a mixture of VO_2 and V_2O_5 phases (Figure 2c). The TEM images (Figure 2d,e) show most of these 2D nanostructures are constituted by multilayered ultrathin nanosheets. We can clearly see from the lateral view of the HRTEM that the thickness of one single layer is about 1.2 nm (Figure 2f). Besides, in the HRTEM image (Figure 2g), the lattice space of 0.204 nm corresponds to the (002) planes of the monoclinic polymorph VO_2 (B) (JCPDS: 31-1439), while the other two sets of lattices with interfringe distances of 0.21 and 0.14 nm correspond to the (110) and (400) planes of the orthorhombic V_2O_5, respectively. The layer-to-layer distance (d-space) is calculated to be 1.38 nm according to the (001) reflection in V_2O_5. The ring-type SAED pattern (see inset in Figure 2g) shows the polycrystalline nature of the nanosheets. The XPS analysis (see Supporting Information Figure S3)

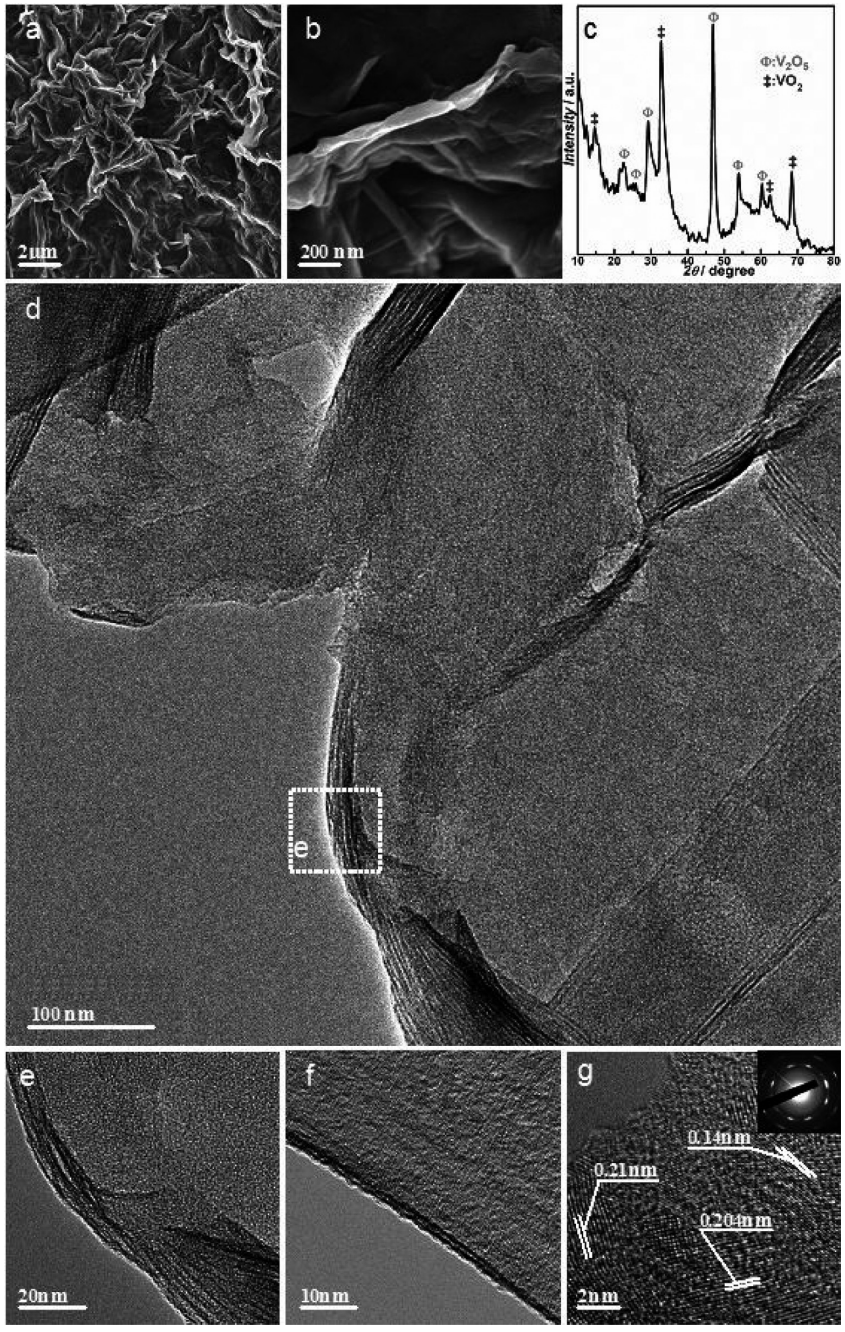

Figure 2. (a) and (b) Low- and high-magnification FESEM images of the 2D nanosheets; (c) XRD patterns; (d) low-magnification TEM images; (e) and (f) high-magnification TEM images; and (g) HRTEM and diffraction patterns (inset).

reveals that the molar ratio of V^{5+}/V^{4+} is around 1.86, indicating that the molar ratio of V_2O_5/VO_2 is 0.93 (i.e., x is about 2.33) in the surface region of the ultrathin VO_x nanosheets. The structure and thickness of the ultrathin nanosheets were further characterized by atomic force microscopy (AFM) analysis. The height of the nanosheets is determined to be 1.2−5.3 nm (Figure 3). The height of the step in the nanosheet is measured to be about 1.2 nm (Figure 3(ii)), which may correspond to the thickness of one single layer of the VO_x nanosheet. Such an observation is consistent with the HRTEM result (Figure 2d,e).

To investigate the formation mechanism of the ultrathin VO_x nanosheets, intermediate products were collected at different reaction times. The TEM images (Figure 4) show the morphology evolution from nanotubes to nanosheets. As reported previously, the multilayer VO_x nanotubes were formed by intercalation of the structure-directing templates (e.g., dodecylamine) into the tube walls,[18] during which process the protonated organic cations (e.g., dodecylamine cations ($C_{12}H_{25}NH_3^+$)) bind electrostatically to the negatively charged VO_x layers.[19] This relatively weak electrostatic interaction provides the possibility to further unfold the multiwall nanotube structure into nanosheets. As we know, dodecylamine cations show good solubility in the acetone solvent. The high-temperature solvothermal process with violent boiling would effectively facilitate the detaching and outward diffusion of the dodecylamine cations from the VO_x tube layers, and the space leaving would be gradually taken by the inward acetone molecules. After 3 h reaction, partial breakage of the nanotubes

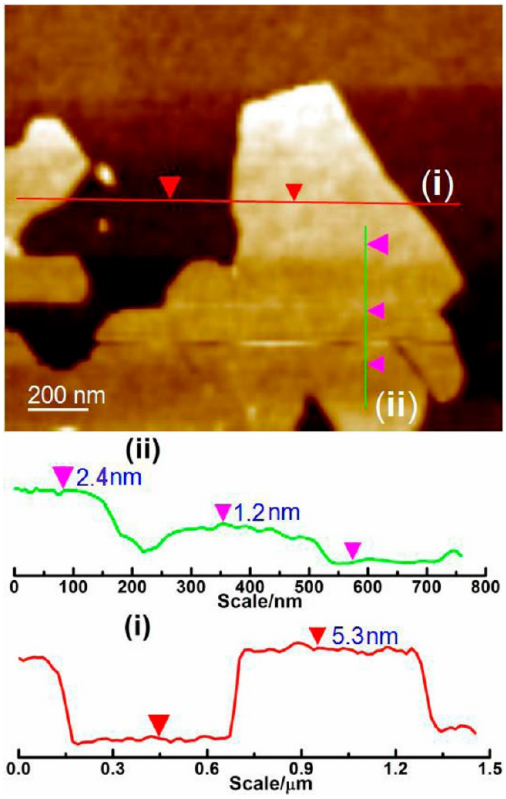

Figure 3. (Top) AFM topography image measured from the nanosheets. (Bottom) The height along the line measured between top and bottom layers in the AFM image.

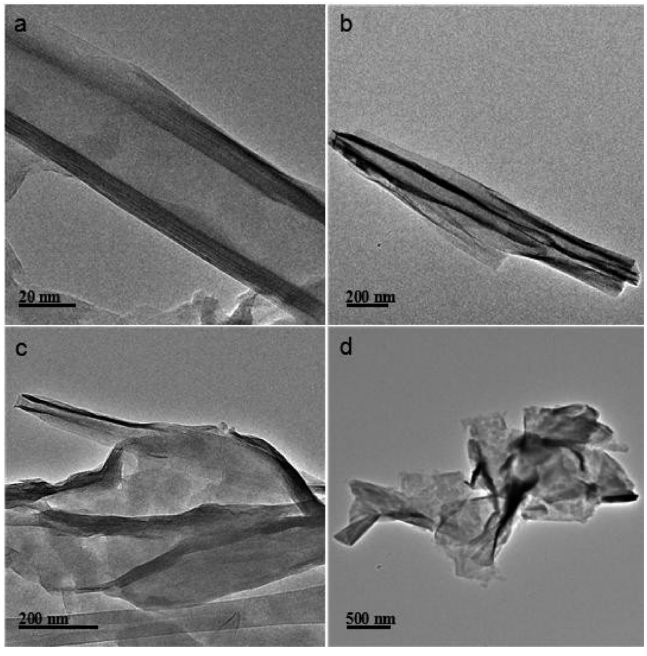

Figure 4. TEM images showing the transformation from nanotubes to nanosheets with time. From (a) to (d): 0 min (multilayer VO_x nanotubes before the diffusion), 3 h, 5 h, and 7 h (ultrathin VO_x nanosheets).

can be clearly observed in the TEM images (Figure 4b). Then, with reaction time increased, more and more hot acetone would immerge into the void space between tube layers from the broken area. As shown in Figure 4c in the Supporting Information, the layered walls of some nanotubes were unfolded to be 2D sheets at a reaction time of 5 h. Further elongation of the reaction time to 7 h would lead to the complete transformation of 1D nanotubes into 2D nanosheets (Figure 4d). In addition, the Fourier transform infrared spectroscopy (FTIR) measurement shows the stretching vibration of terminal oxygen bonds (V═O) and the total disappearance of characteristic peaks of dodecylamine templates in the nanosheets (see Supporting Information Figure S4).[20,21]

The whole transformation process is also illustrated in Figure 1. The specific surface area of these nanosheets was measured by nitrogen adsorption/desorption isotherms and was estimated to be as high as 136.3 $m^2\ g^{-1}$ using the Brunauer–Emmett–Teller (BET) method, which is much higher than that of multilayer VO_x nanotubes (i.e., 25.8 $m^2\ g^{-1}$, see Supporting Information Figure S5). The remarkable increase in surface area upon the structure transformation from nanotube to nanosheet may be related with the peeling process which opens up the surface areas that were overlapped previously in the multilayered tube walls.

Figure 5a,b shows the relationship between the water contact angle (CA) and the time on the surface of the two samples. For the multilayer VO_x nanotube film in Figure 5a, the CA of water is stable and greater than 90° (124 + 1° for the first minute and 116 + 1° for the sixth minute). Therefore, the multilayer VO_x nanotubes can be called hydrophobic nanotubes.[22] However, after solvothermal-induced reaction, a water droplet displays an unstable state on the surface of the ultrathin VO_x nanosheet films (see inset of Figure 5b). The water CA decreased from 129 ± 1° at the first minute to 56 ± 2° at the sixth minute. As we know, if the value of the CA is less than 90°, the surface is hydrophilic.[23] Therefore, the as-obtained ultrathin VO_x nanosheets became hydrophilic.

As shown above, the as-obtained VO_x nanosheets exhibited good hydrophilic property with large specific surface area, which are desirable for a series of applications, e.g., dehydrator, catalyst carrier, gas or liquid purifier, etc. As a demonstration of one potential application, the VO_x nanosheets were used as adsorbent in wastewater treatment. Rhodamine B (RhB), a common azo-dye in the textile industry,[24−26] was chosen as a typical organic waste. When the initial concentration of RhB in water solution was 5 mg L^{-1}, the as-obtained nanosheets could remove about 95% of the RhB within 40 min at room temperature, as shown by the UV/vis absorption curves at different times in Figure 5c,d. When varying the dye concentrations to 15 and 25 mg/L, the removal efficiencies (within 60 min) were 81% and 65%, respectively, based on which we can estimate that maximally 1 g of as-prepared VO_x nanosheets can remove about 60 mg of RhB. Here, the negative zeta potential (−52 mV) and good hydrophilic property of the VO_x nanosheets provide possibility for dye removal, while the unique 2D structures with sufficiently large specific surface area for the electrostatic interaction between the dye molecules and the VO_x nanosheets were supposed to be responsible for the remarkable removal efficiencies. In addition, the VO_x containing RhB could be renewed by catalytic combustion at 200 °C in air for 4 h, and the renewed material kept almost the same adsorption performance (see Supporting Information Figures S6 and S7). Furthermore, as the size of VO_x structures as-prepared was several micrometers, the solid/liquid separation would be fairly easy because they are relatively heavy, which is a very attractive advantage in practical applications.

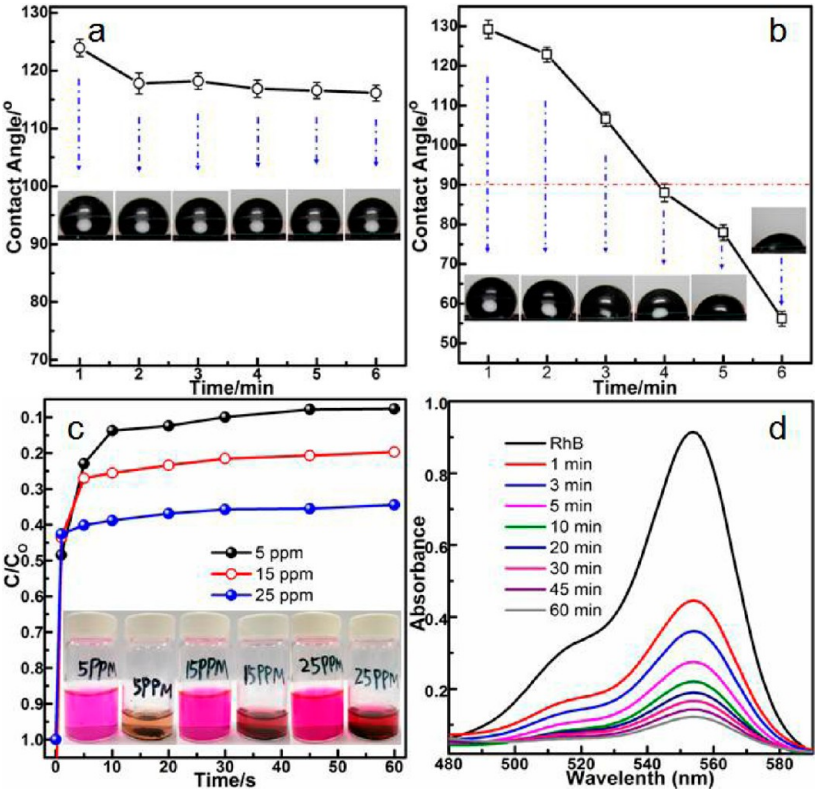

Figure 5. Water CA–time variation for (a) multilayer VO_x nanotube film and (b) ultrathin VO_x nanosheet film on O, flat silicon substrate (shape of a water droplet on the two samples films); (c) adsorption rate of the RhB and photographs after adsorption (inset). C_o (mg/L) is the initial concentration of the RhB solution (i.e., 5, 15, and 20 ppm), and C (mg/L) is the concentration of that at different intervals during the adsorption. (d) Absorption spectra of 10 mL of 5 mg/L RhB solution in the presence of 10 mg of ultrathin VO_x nanosheets in different time.

CONCLUSION

In this work, a useful method for the synthesis of 2D ultrathin VO_x nanosheets was demonstrated based on ultrasonication and solvothermal-induced diffusion. The thickness of the nanosheets is 1.2–5.3 nm from AFM, and BET surface area is ~136.3 m^2 g^{-1}. The as-prepared hydrophilic ultrathin VO_x nanosheet film shows effective water purification capability with RhB adsorption capacity of 60 mg/g, which can be further recycled through a facile combustion process. We believe that this method could be general and applied to the facile production of other novel nanosheets with various potential applications.

ASSOCIATED CONTENT

Supporting Information

Additional figures and table as described in the text. This material is available free of charge via the Internet at http://pubs.acs.org.

AUTHOR INFORMATION

Corresponding Author

*E-mail: alexyan@ntu.edu.sg. Tel.: +65 6790 4583. Fax: +65 6790 9081.

Notes

The authors declare no competing financial interest.

ACKNOWLEDGMENTS

The authors gratefully acknowledge Singapore A*STAR SERC grant 1021700144 and Singapore MPA 23/04.15.03 grant and Singapore National Research Foundation under CREATE program: EMobility in Megacities.

REFERENCES

(1) Wang, Q. H.; Kalantar-Zadeh, K.; Kis, A.; Coleman, J. N.; Strano, M. S. *Nat. Nanotechnol.* **2012**, *7*, 699–712.
(2) Ayari, A.; Cobas, E.; Ogundadegbe, O.; Fuhrer, M. S. *J. Appl. Phys.* **2007**, *101*, 014507–5.
(3) Chen, D.; Feng, H.; Li, J. *Chem. Rev.* **2012**, *112*, 6027–6053.
(4) Pérez-López, B.; Merkoçi, A. *Anal. Bioanal. Chem.* **2011**, *399*, 1577–1590.
(5) Karunadasa, H. I.; Montalvo, E.; Sun, S.; Majda, M.; Long, J. R.; Chang, C. J. *Science* **2012**, *335*, 698–702.
(6) Chianelli, R. R.; Siadati, M. H.; De la Rosa, M. P.; Berhault, G.; Wilcoxon, J. P.; Bearden, R.; Abrams, B. L. *Catal. Rev.* **2006**, *48*, 1–41.
(7) Seo, J. -W.; Jun, Y. -W.; Park, S. -W.; Nah, H.; Moon, T.; Park, B.; Kim, J. -G.; Kim, Y. J.; Cheon, J. *Angew. Chem., Int. Ed.* **2007**, *46*, 8828–8831.
(8) Dean, C. R.; Young, A. F.; Meric, I.; Lee, C.; Wang, L.; Sorgenfrei, S.; Watanabe, K.; Taniguchi, T.; Kim, P.; Shepard, K. L.; Hone, J. *Nat. Nanotechnol.* **2010**, *5*, 722–726.
(9) Radisavljevic, B.; Radenovic, A.; Brivio, J.; Giacometti, V.; Kis, A. *Nat. Nanotechnol.* **2011**, *6*, 147–150.
(10) Liu, W.; Kang, J.; Sarkar, D.; Khatami, Y.; Jena, D.; Banerjee, K. *Nano Lett.* **2013**, *13*, 1983–1990.
(11) Osada, M.; Sasaki, T. *Adv. Mater.* **2012**, *24*, 210–228.
(12) Zeng, Z.; Sun, T.; Zhu, J.; Huang, X.; Yin, Z.; Lu, G.; Fan, Z.; Yan, Q.; Hng, H. H.; Zhang, H. *Angew. Chem., Int. Ed.* **2012**, *51*, 9052–9056.
(13) Son, J. S.; Wen, X. D.; Joo, J.; Chae, J.; Baek, S.-iI.; Park, K.; Kim, J. H.; An, K.; Yu, J. H.; Kwon, S. G.; Choi, S. H.; Wang, Z.; Kim, Y. W.; Kuk, Y.; Hoffmann, R.; Hyeon, T. *Angew. Chem., Int. Ed.* **2009**, *48*, 6861–6864.

(14) Yu, T.; Lim, B.; Xia, Y. *Angew. Chem., Int. Ed.* **2010**, *49*, 4484−4487.
(15) Huang, X.; Tang, S.; Mu, X.; Dai, Y.; Chen, G.; Zhou, Z.; Ruan, F.; Yang, Z.; Zheng, N. *Nat. Nanotechnol.* **2011**, *6*, 28−32.
(16) Feng, J.; Sun, X.; Wu, C.; Peng, L.; Lin, C.; Hu, S.; Yang, J.; Xie, Y. *J. Am. Chem. Soc.* **2011**, *133*, 17832−17838.
(17) Zhou, X.; Wu, G.; Gao, G.; Wang, J.; Yang, H.; Wu, J.; Shen, J.; Zhou, B.; Zhang, Z. *J. Phys. Chem. C* **2012**, *116*, 21685−21692.
(18) Muhr, H. J.; Krumeich, F.; Schönholzer, U. P.; Bieri, F.; Niederberger, M.; Gauckler, L. J.; Nesper, R. *Adv. Mater.* **2000**, *12*, 231−234.
(19) Vera-Robles, L. I.; Campero, A. *J. Phys. Chem. C* **2008**, *112*, 19930−19933.
(20) Surca, A.; Orel, B. *Electrochim. Acta* **1999**, *44*, 3051−3057.
(21) Clauws, P.; Broeckx, J.; Vennik, J. *Phys. Status Solidi B* **1985**, *131*, 459−473.
(22) Feng, X. J.; Jiang, L. *Adv. Mater.* **2006**, *18*, 3063−3078.
(23) Jung, Y. C.; Bhushan, B. *Nanotechnology* **2006**, *17*, 4970−4980.
(24) Stobiecka, M.; Hepel, M. *Phys. Chem. Chem. Phys.* **2011**, *13*, 1131−1139.
(25) Caruana, L.; Costa, A. L.; Cassani, M. C.; Rampazzo, E.; Prodi, L.; Zaccheroni, N. *Colloid Surf. A* **2012**, *410*, 111−118.
(26) Tsukagoshi, K.; Okumura, Y.; Nakajima, R. *J. Chromatogr. A.* **1998**, *813*, 402−407.